INTERNATIONAL SOCIETY FOR SOIL MECHANICS AND GEOTECHNICAL ENGINEERING

The paper was published in the proceedings of the 7th International Conference on Earthquake Geotechnical Engineering and was edited by Francesco Silvestri, Nicola Moraci and Susanna Antonielli. The conference was held in Rome, Italy, 17 – 20 June 2019.

Prediction of liquefaction damage with artificial neural networks

L. Paolella, E. Salvatore, R.L. Spacagna & G. Modoni
University of Cassino and Southern Lazio, Cassino, Italy

M. Ochmański
Silesian University of Technology, Gliwice, Poland

ABSTRACT: The survey of the damage occurred on land, buildings and infrastructures extensively affected by liquefaction, coupled with a comprehensive investigation of the subsoil properties enables to identify the factors that determine the spatial distribution of the phenomenon. With this goal, a database was created in a Geographic Information platform merging records of local seismicity, subsoil layering evaluated by cone penetration tests and groundwater level distribution for the relevant case study of San Carlo (Emilia Romagna-Italy) struck by a severe earthquake in 2012. Here liquefaction phenomena were observed on a portion of the village in the form of sand ejecta, lateral spreading and various damages on buildings and infrastructures. The location of damage allows to test possible relations with the factors characterizing susceptibility, triggering and severity of liquefaction. The relation among the different variables has been herein sought by training a specifically implemented Artificial Neural Network. A relation has thus been inferred between damage and thickness of the liquefiable layer and of the upper crust, seismic input and soil characteristics.

1 INTRODUCTION

Although seismic liquefaction is rarely cause of casualties, it is often responsible for significant economic losses, with serious repercussions on the life of the communities. To reduce economic and social losses and develop plans to mitigate the effects of liquefaction risk assessment procedures have been envisaged (e.g. HAZUS-MH, FEMA 1998). The first step to determine risk is the study of the distribution of hazard on the studied area.

From a mechanical viewpoint, seismic liquefaction is a complex local phenomenon that requires the concomitance of an intense seismic shaking with the presence at shallow depths of loose saturated deposits of sand. The great variety of ground manifestations added to the influence of the soil-building coupling determines the need to analyze the situations with ad hoc models capable of reproducing the role of all factors that determine the triggering and development of liquefaction in the subsoil and, moreover, the interaction between liquefied soil and structures. On the other hand, the quantification of risk at a territorial scale implies the adoption of expeditious solutions, capable of providing answers even with incomplete information. In other words, there is the need to balance accuracy with completeness.

The back-analysis of real examples where the effects of liquefaction have been observed and quantified, coupled with a detailed investigation of the subsoil offers a unique opportunity to establish a relation among the different variables that can be profitably used for risk assessment.

Normally, the quantification of liquefaction severity implies three subsequent stages. A first step is the determination of susceptibility of the subsoil to liquefaction, i.e. the existence of the factors capable of determining the occurrence of liquefaction, without considering specific information on the earthquake but just magnitude. This study, often accomplished in a qualitative way, is sometimes used as a preliminary risk response in some catastrophe models. However, the fact itself that a soil is susceptible to liquefaction does not necessarily imply that

liquefaction will be actually triggered by a seismic event. Therefore, the next step is to determine the likelihood of liquefaction occurrence for given earthquake and subsoil mechanical properties. Magnitude M_w and PGA are normally taken as earthquake parameters for this analysis. During an earthquake, liquefaction is triggered in a soil when the seismic demand, expressed in terms of the cyclic stress ratio (CSR), exceeds the resistance of such soil as expressed by the cyclic resistance ratio (CRR).

The third step consists in assessing liquefaction severity at the ground level (Bird et al., 2006). Several indicators have been proposed in the literature as proxies of the permanent ground deformation (PGDf) and, more generally, of damage. The efficiency of these indicators was tested in specific cases (Bray and Macedo, 2017), but their validity needs to be proved in an enlarged number of case studies, by comparing predictions with observations. Liquefaction severity indicators can also be seen as the "liquefaction demand" for the assessment of the response of the overlying structures and infrastructures, characterized by their own vulnerability. Following the above logic, liquefaction hazard can be defined for a generic structure as the probability that a given value of the liquefaction severity indicator (demand) will be produced during the lifetime of the structure. The practice of characterizing liquefaction hazard through these indicators is applied in many countries to quantify risk on structures and infrastructures present in a given territory (e.g. DPC 2017, MBIE 2016, Yasuda and Ishikawa, 2018).

1.1 Liquefaction severity indicators

For a given soil profile, the triggering of liquefaction at different depths can be evaluated by applying several approaches. One of the most popular is the cyclic stress approach, which implies the calculation of a liquefaction safety factor (FSL), obtained by dividing the cyclic stress ratio τ/σ'_v producing liquefaction (CRR) with the one induced by the earthquake (CSR).

Boulanger and Idriss (2014) provide an empirical formulation of the Cyclic Resistance Ratio based on the survey of liquefaction and the results of common geotechnical and geophysical in-situ tests (CPT, SPT, Vs profile). A simplified method to estimate the CSR profile was developed by Seed and Idriss (1971) based on the maximum ground surface acceleration (a_{max}) at the site.

$$CSR = 0.65 * \left(\frac{a_{max}}{g}\right) * \left(\frac{\sigma vo}{\sigma vo\prime}\right) * r_d \tag{1}$$

in which σ_v and σ'_v represent respectively the total and effective vertical stress at a depth z, a_{max}/g is the maximum horizontal acceleration (as a fraction of gravity) at the ground surface and r_d is the shear stress reduction factor that accounts for the dynamic response of the soil profile.

Once the Factor of Safety has been calculated at each depth, synthetic indicators of the liquefaction severity on the ground (free field) are provided.

In general terms, a liquefaction severity indicator can be defined as the integral of the product between a function of the Factor of Safety against Liquefaction f_l(FSL) and a weight function that emphasizes the severity of liquefaction at a lower depth.

$$INDEX = \int_{z_{min}}^{z_{max}} f_1(FSL) * w(z) dz \tag{2}$$

In Table 1, the two functions f_l(FSL) and w(z) and the limits of integration are defined for the most commonly used liquefaction severity indicators.

1.2 Ishihara's methodology

Ishihara and Ogawa (1978) used borehole data from sites where liquefied material ejection at the ground surface was observed after past earthquakes to develop a general relationship

Table 1. The most widespread indicators, except the LDI which was defined for lateral spreading, quantify the damage to the ground by integrating the estimated effects of liquefaction in the first 20 m depth.

INDEX	REFERENCE	$f_1(FSL)$	$w(z)$	Z
LPI	Iwasaki, 1978	$1 - FSL$ if FSL < 1 0 if $FSL1$	$10 - 0.5z$	$Z_{min} = 0$ $Z_{max} = 20\ m$
LPI_{ISH}	Maurer, 2014	$\begin{cases} 1 - FSL & if & FSL \leq 1 \cap^{H_1} \cdot m(FSL) \leq 3 \\ 0 & otherwhise \end{cases}$ Where: $m(FSL) = \exp\left(\frac{5}{25.56(1-FSL)}\right) - 1$	$\dfrac{25.56}{z}$	$Z_{min} = H_1$ $Z_{max} = 20\ m$
W	Zhang et al., 2002	$\varepsilon_v = \varepsilon_v\ (FSL, qc_{1Ncs})$	-	$Z_{min} = 0$ $Z_{max} = \max depth$
LDI	Zhang et al., 2004	$\gamma_{max} = \gamma_{max}\ (FSL,\ qc_{1N})$	-	$Z_{min} = 0$ $Z_{max} < 23\ m$
LSN	van Ballegooy, 2014	$\varepsilon_v = \varepsilon_v\ (FSL, qc_{1Ncs})$	$\dfrac{1000}{z}$	$Z_{min} = 0$ $Z_{max} = 20\ m$

linking the thickness of non-liquefying material (H1) and the underlying thickness of liquefied stratum (H2) to the manifestations at the ground surface. In particular, in the three-strata model defined by Ishihara, the liquefiable layer is identified by loose saturated sands having N_{SPT} less than 10.

Considering the importance of the non-liquefied capping layer, H_1, and the liquefied strata thickness, H_2, Ishihara (1985) proposed boundary curves for predicting liquefaction manifestation as a function of H_1, H_2 and peak ground acceleration. As shown in Figure 1: for a given PGA, there is a limiting value of the non-liquefiable crust thickness beyond which surface manifestations do not form regardless of H_2. It means that the liquefied deposit must be both of sufficient thickness and close enough to the ground surface for the resulting excess pore water pressure to rupture the ground surface.

Based on Ishihara's experiences and supported by the numerical modeling of the phenomenon, an alternative CPT-based method to quantify the liquefaction hazard is herein proposed and applied. In fact, since the numerical models show that the triggering of liquefaction in the deepest layer prevents the development of the phenomenon in the upper layers, a CPT profile can be processed following a bottom-up approach (Figure 2). This allows to obtain a simplified three-strata model, by isolating the deepest liquefiable layer (i.e. where the Factor of Safety is found less than 1 for at least 1 m) and considering all the superior layers as crust (H_1). In addition to the crust thickness (H_1), the thickness (H_2) and the mean Factor of Safety are evaluated for the liquefiable layer thus identified.
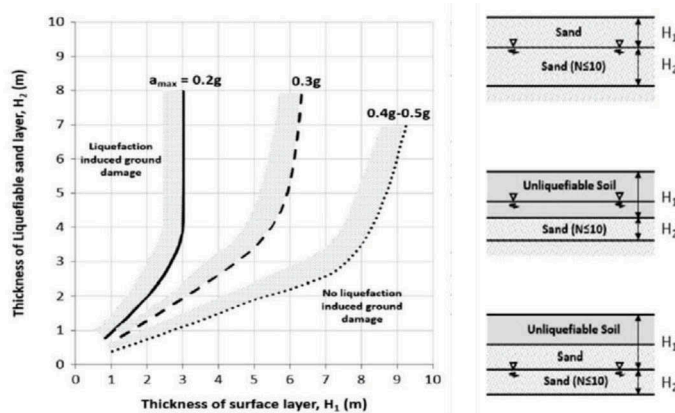

Figure 1. Ishihara boundary curves and criteria to define H_1 and H_2 for a soil profile (Maurer, 2014).
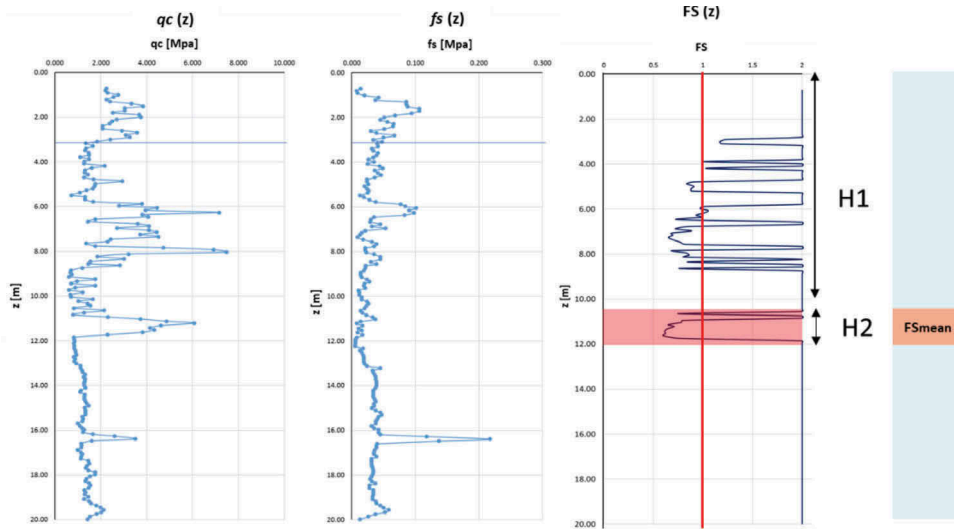
Figure 2. Schematic procedure to obtain the simplified three-strata model from CPTs, analyzed following a bottom-up approach.

2 ARTIFICIAL NEURAL NETWORKS

In practical applications where data management and interpretation are required for a significant amount of information, especially in cases where complex (e.g. non-linear) relationships exist between variables, Artificial Neural Networks (ANNs) represent a powerful tool able to establish a link between input datasets and output. The basic principle of ANN is that the mathematical connection between the variables is not given a priori but is established training data which can come from real examples. The idea behind an ANN is to produce a machine or a model that simulates the learning capacity of a human brain, seen as a non-linear and highly parallel computer which organizes its elementary units (neurons) in order to carry out some types of calculations (daily actions).

Similarly, artificial neural networks are constituted by the interconnection of elementary computational units (called neurons) having two fundamental characteristics: 1) knowledge is acquired from the environment through a process of learning or training; 2) the knowledge is stored in the parameters of the network and, in particular, in the weights associated with the connections.

Neurons, on the other hand, are defined as nodes of a geared network provided with processing capacity. Some neurons receive information from the outside (input unit), others emit responses to the outside (output unit) and a third group still communicate only with the internal elements of the network (hidden units). Each unit becomes active if it receives a quantity of signal that exceeds its activation threshold. After that, this unit emits a new signal to the surrounding units to which it is connected, through the connection points. These act as weight, amplifying or reducing the intensity of the received signal according to their individual characteristics (Floreano and Mattiussi, 2002).

The response signal emitted by a node (n_i) can be described as a function Φ of the sum of the products of all input signals (n_j) for the respective weights (w_{ij}) minus the value of the activation threshold (θ_i).

$$n_i = \Phi\left(\sum_j w_{ij}n_j - \theta_i\right) \tag{3}$$

One of the most important properties of artificial neural networks is generalization. In fact, once the network has been appropriately trained on a limited number of models, it is possible

to apply it to a potentially infinite number of input combinations. This capability, together with the development of the backpropagation algorithm (Rumelhart et al., 1986), has significantly extended the field of application of ANN not only in computer science and control systems but also in engineering, medical and statistical applications.

3 APPLICATION OF ANN'S TO LIQUEFACTION HAZARD ASSESSMENT

Past studies (Goh, 2002; Ülgen and Engin, 2007) shown that ANNs can also be exploited in the prediction of liquefaction-induced damage on the ground. In particular, Kurup and Dudani (2001) focused on the use of the backpropagation algorithm to evaluate the liquefaction potential starting from CPTs. This possibility is now enhanced by the tendency to create rich databases including the results of subsoil investigations collected at a local or regional scale. These data can be profitably coupled with the survey of damage achieved in cases where liquefaction has occurred to train the ANNs and establish a logical connection between severity factors and damage.

Following the recent major seismic events that produced significant liquefaction damage, such as the 2010-2011 and 2016 Christchurch (New Zealand) earthquakes, the 2012 Emilia-Romagna (Italy) earthquake, the 2016 Kumamoto (Japan) earthquake, the scientific community has decided to support reconstruction strategies by establishing databases in order to facilitate the data sharing among the stakeholders and to support the post-earthquake, political and economic evaluations. One of the most important examples is the Canterbury Geotechnical Database CGD, established and founded by the New Zealand Government (MBIE) and the Earthquake Commission (EQC), after the 2010-2011 Christchurch earthquake Sequence that was characterized by 5 major shocks with extensive evidence of liquefaction. For the Emilia-Romagna Region, a large amount of geological-technical data was already available in numerous and fragmented archives of public and private property, collected to support cognitive investigations of various nature. In recent years, the Region encouraged the collection of the existing data and their loading into numerical archives, that are constantly updated. After the May-June 2012 seismic sequence, a considerable amount of new geotechnical information and surveys, coming from the report prepared for the reconstruction of buildings have been added to the already existing information. The Geotechnical Database includes, at January 2018, more than 85 000 publicly available tests.

3.1 The case study of S. Carlo

The San Carlo district of the municipality of Sant'Agostino (Italy) was hit by the May-June 2012 seismic sequence, which main event was the M_w 5.9 20th May earthquake, characterized by huge building damage (around 200 buildings suffered different levels of damage only in San Carlo district) and extensive liquefaction (sand boils and cracks). Geological features of the area and past studies (Galli and Meloni, 1993; Romeo, 2012), highlight the presence of numerous paleochannels where different lithologies, constituting the alluvial plain, can be found. In particular, it can be observed that almost the entire municipality of Terre del Reno is located along the old Reno River, where the most of liquefaction-induced phenomena was observed (Figure 3a).

For the study area of S. Carlo, the map of liquefaction evidence (on both ground and buildings) was converted in terms of liquefaction severity classes. A regular grid of 25x25 meters covering the municipality was considered; then, it was possible to estimate the severity of liquefaction-induced damage as a function of the distance between each centroid and the liquefaction evidence (Figure 3b).

3.2 Example of analysis

Considering the district of S. Carlo, around 200 CPTs were processed. The analysis of the traditional liquefaction hazard, carried out on the entire municipality of Terre del Reno, is reported here for the (M_w 5.9) 20 May 2012 earthquake. The factor of safety was evaluated by applying the Boulanger & Idriss (2014) procedure, while, in addition to the traditional "LPI" index, the
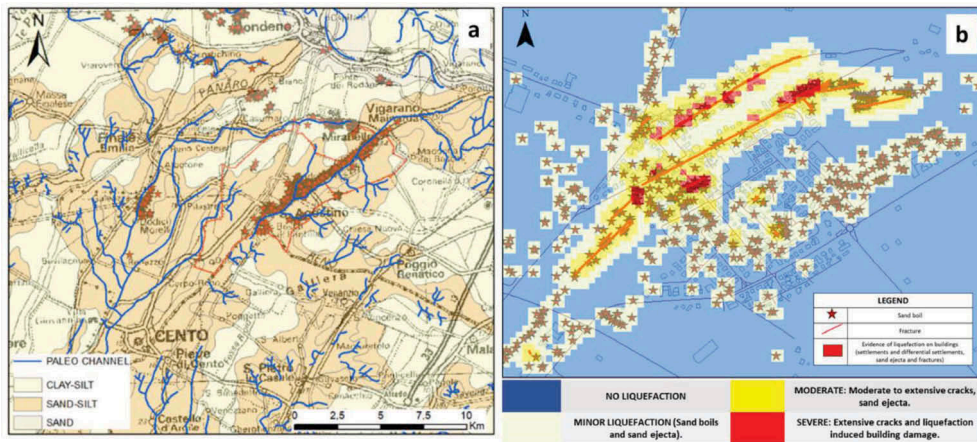
Figure 3.   a) Paleochannels and alluvial deposits present in the study area; red stars represent the localized liquefaction ground observations; b) Liquefaction ground observations after the 20 May 2012 earthquake.

Ishihara inspired "LPI$_{ISH}$" (Maurer, 2014) was also calculated. The values of such indicators were then interpolated through geostatistical analysis to obtain maps of liquefaction severity. An example is the map of the "LSN", shown in Figure 4, that highlights a heterogeneous distribution of values in the area with a concentration of potentially liquefiable layers, corresponding to LSN > 20-25, along the Reno River Paleochannel. This trend is strongly influenced by the geology of the area consisting mainly of modern alluvial deposits (Figure 3a).

The bottom-up analysis of the available CPTs showed that for the selected study area, the mean factor of safety against liquefaction ranges between 0.1 and 0.7, while no liquefiable layers thicker than 8 m were evaluated. In order to find a correlation between the prediction and surficial observation of liquefaction-induced phenomena, an Artificial Neural Network was trained (Figure 5). In particular, the backpropagation algorithm was applied to an architecture consisting of one hidden layer and one hundred neurons. This architecture was found with a trial and error process to give the best compromise between computational effort and the quality of output. The evaluated H_1, H_2 and FSm represent the input variables and the respective liquefaction damage level is the output, assuming a value of 1.75 as a threshold of
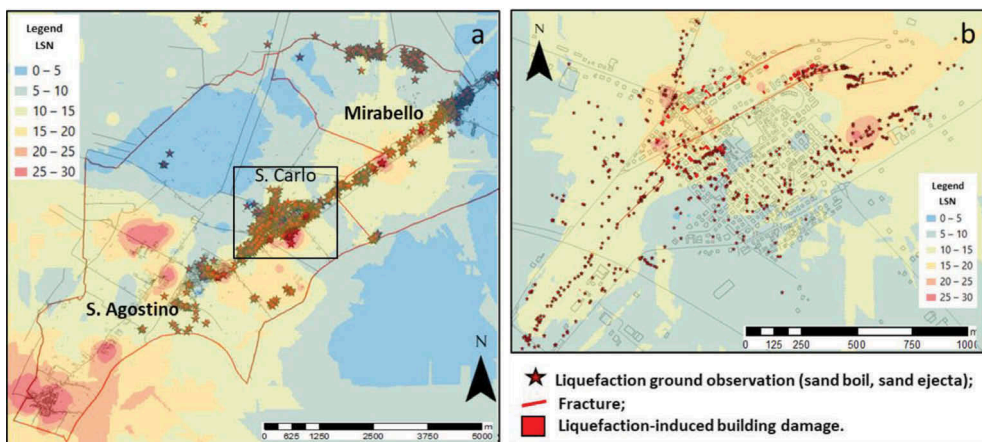

Figure 4.   Geostatistical interpolation of "LSN" on the entire municipality of S. Agostino and Mirabello (a) and on the district of S. Carlo (b), with liquefaction ground observations and liquefaction-induced building damage.
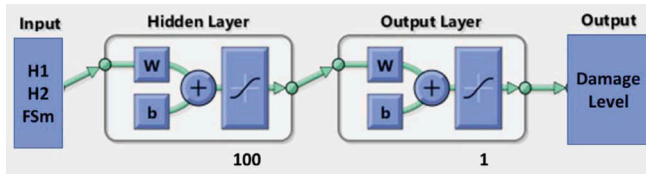
Figure 5. Simplified scheme of functional relationships between input (H_1, H_2 and mean factor of safety) and output (Liquefaction damage level) data of the artificial neural network.

liquefaction-induced damage. For the case below mentioned, a binary classification of damage/no damage was applied.

Once the neural network was trained and validated (with a reliability coefficient equal to 0.85), it was tested on 10 000 random combinations of the input values to represent a more extensive and generalized case series. The obtained results were plotted on the plane H_1, H_2 for given values of the mean Factor of Safety (FSm), ranging in 0.2 and 0.9 values (Figure 6). This allowed to separate, for each class of FSm, the liquefiable domain (i.e. above the limit curve) from the region where surficial liquefaction observations are unlikely (i.e. below the limit curve).

3.3 Conclusions

Given the nature of liquefaction and its impact on a community, seismic and liquefaction risk assessment must be undertaken to reduce the total economic loss. The first step of such analysis is the characterization of the hazard. Since liquefaction is governed by non-linear relationships between the involved variables, artificial neural networks (ANNs) can be a useful alternative to traditional indicators in predicting the liquefaction severity on the ground. In this work, for the case study of S. Carlo (2012 Emilia earthquake, M_w 5.9), liquefaction hazard was assessed both through the traditional severity indicators (LPI, LSN, post-liquefaction settlement) and on the basis of a new approach inspired by Ishihara and the numerical models of liquefaction. Thus, a neural network was trained for binary classification (damage/no damage) on the district of S. Carlo and curves that relate the thickness of the non-liquefying crust (H_1) to the thickness of the liquefiable layer (H_2), as a function of the mean factor of safety, are proposed. However, the effectiveness of the procedure must be confirmed by the extension of the study area to the whole municipality of Terre del Reno and by the consideration of new case studies.
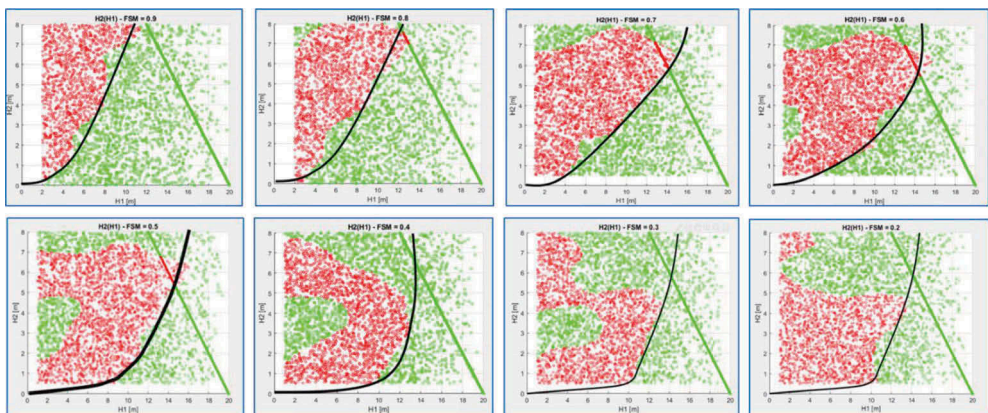

Figure 6. Relationship between the crust thickness (H_1) and the liquefiable thickness (H_2) as a function of the mean factor of safety (FSm) for sites where ground liquefaction occurred during the 20 May 2012 earthquake, after the training of an ANN for the selected study area.

ACKNOWLEDGEMENT

REFERENCES

Bird, J. F., Bommer, J. J., Crowley, H. & Pinho, R. 2006. Modelling liquefaction-induced building damage in earthquake loss estimation. Soil Dyn. Earthq. Eng. 26: 15–30.

Boulanger, R.W. & Idriss, I.M. 2014. CPT and SPT based liquefaction triggering procedures. Department of Civil and Environmental engineering, University of California at Davis.

Dipartimento della Protezione Civile "DPC" 2017. Linee guida per la gestione del territorio in aree interessate da liquefazioni (LQ). Versione 1.0. Roma 2017.

Bray, J. D. & Macedo, J. 2017. Simplified procedure for estimating liquefaction-induced building settlement. *Proceedings of the 19th International Conference on Soil Mechanics and Geotechnical Engineering*, Seoul 2017

FEMA/NIBS 1998. HAZUS - Earthquake Loss Estimation Methodology. Vol. 1, 1998.

Floreano, D. & Mattiussi, C. 2002. Manuale sulle reti neurali - Seconda edizione, 2002. Società editrice: Il Mulino, Bologna.

Galli, P. & Meloni, F. 1993. Liquefazione Storica. Un catalogo nazionale. Quat. Ital. J. Quat. Sci. 6. Pagg. 271–292.

Goh, A. T. C. 2002. Probabilistic neural network for evaluating seismic liquefaction potential. Canadian Geotechnical Journal. 39: 219–232 (2002).

Ishihara, K. & Ogawa, K. 1978. Liquefaction susceptibility map of downtown Tokyo. Proceedings of the 2nd international conference on microzonation for safer construction. Vol.2; 1978. p.897–910.

Ishihara, K. 1985. Stability of Natural Deposits During Earthquakes Proceedings of the 11th International Conference on Soil Mechanics and Foundation Engineering, San Francisco, 1:321–376.

Iwasaki, T., Tatsuoka, F., Tokida, K. & Yasuda, S. 1978. A Practical method for assessing soil liquefaction potential based on case studies at various sites in Japan. [conference]: 2nd International conference on Microzonation. - 1978: 885–896.

Kurup, P. U. & Dudani, N. K. 2001. CPT Evaluation of Liquefaction Potential Using Neural Networks. International Conferences on Recent Advances in Geotechnical Earthquake Engineering and Soil Dynamics. 28.

Maurer, B. W., Green, R. A., Oliver, S. & Taylor, O. S. 2014. Moving Towards an Improved Index for Assessing Liquefaction Hazard: Lessons from Historical Data. Soils and Foundations, 55(4): 778–787.

Ministry of Business, Innovation & Development – NZGS, 2016. Recommendation after the Canterbury Earthquake sequence (2010–2011).

Robertson, P. 1990. Soil classification using the cone penetration test. Canadian Geotechnical Journal, 27(1):151–158.

Romeo, R.W. 2012. Emilia (Italy) M5.9 earthquake on 20 May 2012: an unusual pattern of liquefaction. Italian Journal of Engineering Geology and Environment, 2 (2012).

Rumelhart, D. E., Hinton, G. E. & Williams, R. J. 1986. Learning Representations by Back-Propagation of errors. Nature, vol. 323: 533–536.

Seed, H.B & Idriss, I.M. 1971. Simplified procedure for evaluating soil liquefaction potential. Journal of the Soil Mechanics and Foundations Division. ASCE 97(SM9): 1249–1273.

Università degli Studi di Ferrara, Dipartimento di Fisica e Scienze della Terra, 2014. Microzonazione sismica del Comune di Sant'Agostino.

Ülgen, D & Engin, H. K. 2007. A study of CPT based liquefaction assesment using ANN. 4th International Conference on Earthquake Geotechnical Engineering. June 25–28, 2007.Paper No. 1219.

van Ballegooy, S., Malan, P., Lacrosse, V., Jacka, M.E., Cubrinovski, M., Bray, J.D., O'Rourke, T.D., Crawford, S.A. & Cowan, H. 2014. Assessment of Liquefaction-Induced Land Damage for Residential Christchurch. Earthquake Spectra (30) No. 1: pages 31–55, February 2014.

Yasuda, S. & Ishikawa, K. 2018. Liquefaction-induced Damage to Wooden Houses in Hiroshima and Tokyo during Future Earthquakes. 16 ECEE, Thessaloniki, Greece, June 2018.

Zhang, G., Robertson, P.K. & Brachman, R.W.I. 2002. Estimating liquefaction-induced ground settlements from CPT for level ground. Canadian Geotechnical Journal 39: 1168–1180.

Zhang, G., Robertson, P.K. & Brachman, R.W.I. 2004. Estimating liquefaction-induced Lateral Displacements from CPT for level ground. J. of Geotech. and Geoenvironmental Engineering. AUGUST 2004.